Mesoporous Matrix Encapsulation for the Synthesis of Monodisperse Pd$_5$P$_2$ Nanoparticle Hydrodesulfurization Catalysts

Galbokka H. Layan Savithra,[†] Richard H. Bowker,[‡] Bo A. Carrillo,[‡] Mark E. Bussell,[‡] and Stephanie L. Brock*,[†]

[†]Department of Chemistry, Wayne State University, Detroit, Michigan 48202, United States
[‡]Department of Chemistry, Western Washington University, Bellingham, Washington 98225-9150, United States

S *Supporting Information*

ABSTRACT: The synthesis of monodisperse 5−10 nm Pd$_5$P$_2$ catalytic particles by encapsulation in a mesoporous silica network, along with preliminary data on hydrodesulfurization (HDS) activity, is reported. Precursor Pd−P amorphous nanoparticles are prepared by solution-phase reaction of palladium(II) acetylacetonate with trioctylphosphine at temperatures up to 300 °C. Direct crystallization of Pd$_5$P$_2$ in solution by increasing the temperature to 360 °C leads to sintering, but particle size can be maintained during the transformation by encapsulation of the amorphous Pd−P

particles in a mesoporous silica shell, followed by treatment of the solid at 500 °C under a reducing atmosphere, yielding Pd$_5$P$_2$@ mSiO$_2$. The resultant materials exhibit high BET surface areas (>1000 m^2/g) and an average pore size of 3.7 nm. Access to the catalyst surface is demonstrated by dibenzodithiophene (DBT) HDS testing. Pd$_5$P$_2$@mSiO$_2$ shows a consistent increase in HDS activity as a function of temperature, with DBT conversion approaching 60% at 402 °C. The ability to control particle size, phase, and sintering is expected to enable the fundamental catalytic attributes that underscore activity in Pd$_5$P$_2$ to be assessed.

KEYWORDS: *Pd$_5$P$_2$ nanoparticle synthesis, mesoporous silica, HDS catalysis, dibenzothiophene, sintering prevention*
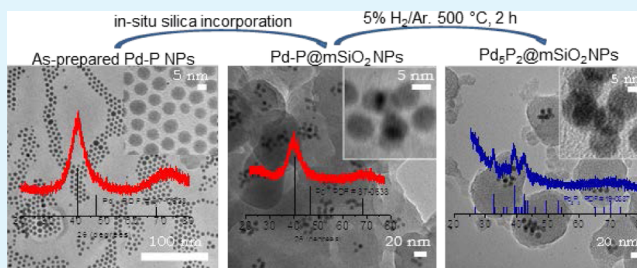
T o minimize damage to the environment and to human health, the United States and other countries have implemented environmental regulations lowering the allowable sulfur content in highway diesel fuel from 500 to 15 ppm over the last two decades, and further reductions (upper limit of 5− 10 ppm) are expected in the near future.[1] To meet these standards, we need to develop processes for efficiently removing the most refractory sulfur compounds, such as 4,6 dimethyldibenzothiophene (4,6-DMDBT), from crude oil. The very low reactivity of these refractory sulfur compounds is due to steric hindrance limiting access to the C−S bond.[2−5] Removal of refractory sulfur occurs more efficiently by a hydrogenation (HYD) pathway, wherein hydrogenation of a phenyl group occurs first, deplanarizing the ring and enabling access to the sulfur center, as opposed to direct attack at sulfur (direct desulfurization (DDS)). As a result, noble metals such as Pd, Pt, and Rh, which are excellent hydrogenation catalysts, show high activity for deep-HDS when dispersed as nanoscale particles on an oxide support.[6−9] However, noble metals are susceptible to sulfur poisoning, causing the activity to drop over time. This problem has been addressed by the use of noble metal phosphides (Rh$_2$P,[10−12] Ru$_2$P,[12−14] Pd$_5$P$_2$[12,13]) prepared by the temperature programmed reduction method (TPR). Phosphides are more resistant to sulfur poisoning while maintaining good HDS activity. For example, Rh$_2$P catalysts showed higher dibenzothiophene (DBT) HDS activity compared to commercial Ni−Mo/Al$_2$O$_3$ and Rh/SiO$_2$ catalysts

and are sulfur tolerant (stable over 100 h of DBT HDS).[10] Pd phosphides (e.g., Pd$_5$P$_2$) on silica have also exhibited promising HDS properties, with activities between those of Ru phosphides (Ru$_2$P, RuP) and Rh$_2$P.[12,13] However, size-dependent activity relationships have not been established for these materials because the TPR method results in polydisperse samples with little control over particle size and shape.[15]

The direct synthesis of monodisperse, spherical, small (5−10 nm) noble metal phosphide nanoparticles has proven challenging to achieve by solution phase arrested precipitation. For the case of Pd$_5$P$_2$, the focus of the present study, it has been shown that premade Pd nanoparticles will react with TOP at 330 °C, resulting in a mixture of Pd$_5$P$_2$ and PdP$_2$.[16] Phase-pure Pd$_5$P$_2$ particles were successfully prepared from the direct reaction between palladium(II)acetylacetonate (Pd(acac)$_2$) with TOP.[16] However, the particle size and distribution were not quantified. Pd$_5$P$_2$ nanoparticles can also be prepared by reaction of Pd nanoparticles with stoichiometric amounts of white phosphorus, P$_4$.[17] In this case, the product particles appear to retain a significant amorphous component and are irregular in shape and polydisperse in size (5−20 nm). Here we demonstrate that phase-pure monodisperse samples of 5−10

nm Pd_5P_2 can be prepared by encapsulation of amorphous Pd–P particles in a mesoporous silica shell prior to crystallization. The shell limits sintering, yet enables access to the particle surface, as demonstrated by HDS catalytic testing.

Precursor amorphous Pd–P particles were prepared by reaction of 0.33 mmol of $Pd(acac)_2$ with 5 mL of TOP (P:Pd = 34) in the presence of 2–5 mL of oleylamine and 10 mL of octylether at varying temperatures (270–300 °C) for 0.5–12 h. Two broad peaks in the powder X-ray diffraction (PXRD) pattern reveal the amorphous nature of the resultant product even after 12 h at 300 °C (Figure 1a). EDS analysis performed
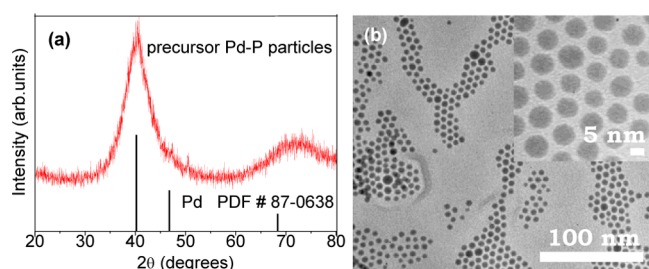
Figure 1. (a) Powder X-ray diffraction (PXRD) pattern and (b) TEM image of Pd–P nanoparticles formed using 5 mL of oleylamine at 300 °C for 2 h.

on these amorphous products reveals that these particles have a significant level of P (the Pd:P ratio varies between 50:50 and 70:30) incorporated into the palladium lattice (see Figure S1 in the Supporting Information). This observation is in agreement with the nickel phosphide system where Ni–P amorphous nanoparticles are generated when a large amount of TOP is used at moderately high temperatures (230–260 °C).[18,19] While there is no direct evidence of an amorphous Pd–P alloy, EXAFS analysis of Ni–P amorphous alloys show that P is substitutionally incorporated into the Ni lattice,[20] and we surmise Pd behaves similarly. The Pd–P amorphous nanoparticles are spherical and nearly monodisperse (9 ± 0.9 nm), self-assembling into a hexagonal pattern (Figure 1b). The average particle size of Pd–P can be tuned by varying the amount of oleylamine; the average particle size increases from 6 to 9 nm when the amount of oleylamine in the reaction is increased from 2 to 5 mL (see Figure S2 in the Supporting Information). This Pd–P amorphous particle size dependency on amount of oleylamine is consistent with the Ni–P amorphous particle system.[21]

When the reaction was carried out at 360 °C for 1 h, the presence of crystalline Pd_5P_2 was observed by PXRD (see Figure S3 in the Supporting Information). However, a broad feature was present beneath the sharp Pd_5P_2 peaks, suggesting that amorphous Pd–P was also present. If instead heated for 2 h at 360 °C, phase-pure PdP_2 was formed and the PXRD peaks are sharp, indicating that the crystallites are quite large in size. These observations are similar to those noted by Carenco et al.[17] To prevent formation of the phosphorus-rich phase PdP_2, we reduced the amount of TOP systematically and found that phase-pure Pd_5P_2 is formed when only 1 mL (P:Pd = 6.8) instead of 5 mL of TOP (P:Pd = 34) is employed at a reaction temperature of 360 °C after 4 h (Figure 2a). Under these conditions, nucleation (as probed by a change in color of the solution) did not take place below 360 °C suggesting Pd–P amorphous particles were not formed as intermediates. Instead, formation of crystalline Pd_3P occurs first (dominant phase) at
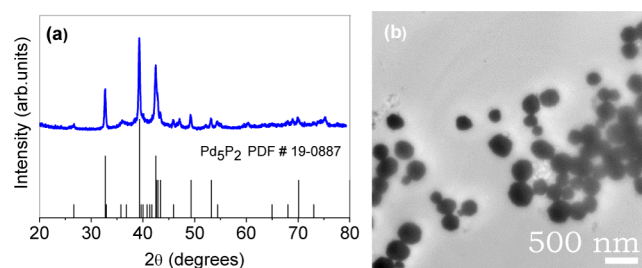
Figure 2. (a) PXRD pattern and (b) TEM image of Pd_5P_2 particles made by direct reaction of $Pd(acac)_2$ and TOP (P:Pd = 6.8) at 360 °C for 4 h.

360 °C (within 1 h of the reaction) followed by the conversion to Pd_5P_2 (see Figure S4 in the Supporting Information, Figure 2a). The EDS analysis performed on Pd_5P_2 suggested a Pd:P ratio of 70.6:29.4, which is close to the theoretical value (71.4:28.6, see Figure S4 in the Supporting Information). However, the Pd_5P_2 crystallites were large and aggregated, yielding clusters a few hundred nm in diameter, as shown by TEM analysis (Figure 2b), and as reflected in the narrow peak widths in the PXRD pattern (Figure 2a).

To prevent sintering in the formation of Pd_5P_2, we developed a novel synthetic strategy in which intermediate monodisperse discrete Pd–P nanoparticles formed at 300 °C (avoiding the formation of PdP_2) were trapped in a mesoporous silica network and then converted to the catalytically interesting phase, Pd_5P_2, by heating under reducing conditions in a flow furnace.

Phase transfer of Pd–P nanoparticles to water was achieved by addition of chloroform-dispersed Pd–P nanoparticles into a concentrated cetyltrimethylammonium bromide (CTAB) aqueous solution followed by evaporation of chloroform at 75 °C for 20–30 min. Subsequently, base-catalyzed silica polymerization was performed by injecting tetraethylorthosilicate (TEOS) to the basified Pd–P/CTAB/H_2O solution resulting in Pd–P@$mSiO_2$. TEM reveals discrete, spherical, and monodisperse Pd–P particles embedded in a mesoporous silica matrix (Figure 3b) and the particles remain amorphous during the encapsulation process (compare Figures 1a and 3a).

To remove the template (CTAB) and crystallize the amorphous Pd–P alloy to form Pd_5P_2, we attempted a two-step process: calcination in air to remove CTAB followed by reduction to form the phosphide. Prior attempts with Ni_2P to remove the template under reducing conditions always led to formation of more Ni-rich products (Ni_3P and $Ni_{12}P_5$), suggesting carbothermal reduction of Ni_2P is occurring.[21] Accordingly, calcination of Pd–P@$mSiO_2$ was performed at 430 °C in air for 2.5 h to remove the CTAB template and organic ligands bound to the nanoparticle surface. This resulted in formation of PdO@$mSiO_2$ in which PdO is the only crystalline product detected (see Figure S5b in the Supporting Information). Attempts to recover the phosphide by heating PdO@$mSiO_2$ in a flowing 5% H_2/Ar mixture at temperatures up to 650 °C for 2 h yielded only the Pd phase (see Figure S5c in the Supporting Information). These data suggest that either the oxidized phosphorus species do not convert to a more reduced state under these conditions or that phosphorus is lost during calcination. Because PPh_3 has proven to be a useful phosphorus source in metal phosphide synthesis, including to achieve Ni_2P in post-oxidized Ni_2P@$mSiO_2$,[18,21–24] we introduced PPh_3 vapor by placing a sample of solid PPh_3
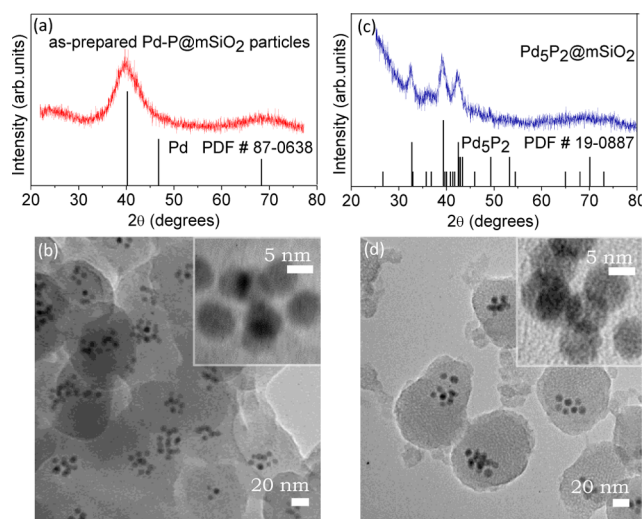
Figure 3. PXRD patterns of (a) as-prepared Pd−P@mSiO$_2$ nanoparticles and (c) 5 wt % Pd$_5$P$_2$@mSiO$_2$ nanoparticles formed after treating as-prepared Pd−P@mSiO$_2$ nanoparticles under 5% H$_2$/Ar mixture at 500 °C for 2 h; corresponding TEM images (b) Pd−P@mSiO$_2$ and (d) Pd$_5$P$_2$@mSiO$_2$.

upstream of the oxidized Pd-P@mSiO$_2$ sample in the flow furnace and, under reducing conditions, varying the temperature and time. As the temperature was increased to 650 °C, the phase transformation from Pd to Pd$_5$P$_2$ took place gradually via the intermediate Pd−P amorphous phase (see Figure S5d−f in the Supporting Information). However, the peaks remain very broad, suggesting that the majority of the sample remains amorphous.

We next attempted directly heating as-prepared Pd−P@mSiO$_2$ particles under a 5% H$_2$/Ar mixture at 500 °C for 2 h in a flow furnace. In contrast to Ni$_2$P@mSiO$_2$ (vide supra),[21] a complete transformation from amorphous Pd−P to phase-pure Pd$_5$P$_2$ was observed without loss of P (Figure 3c). This is attributed to the solid state transformation (reduction) and reorganization (crystallization) of phosphorus present in Pd−P particles to Pd$_5$P$_2$, and the resistance of this phase to carbothermal reduction. Most importantly, the particles retain their morphology (spherical) and do not appear to sinter (Figure 3d); rather the particles are localized/embedded at different levels within the mesoporous silica particles. Morover, the particles appear to be similar in size to the Pd−P precursor, 8.2 ± 0.7 nm by Scherrer analysis of PXRD data in Figure 3c and EDS analysis performed on this sample revealed that the Pd:P ratio (71.2:28.8) is in close agreement with the theoretical ratio (71.4:28.6) of Pd$_5$P$_2$ (see Figure S6 in the Supporting Information). The final Pd$_5$P$_2$@mSiO$_2$ weighed ∼750−800 mg, indicating that silica polymerization goes to completion (theoretical yield of silica ∼740 mg and Pd$_5$P$_2$ ∼39 mg). Notably, even when the precursor Pd−P particles are P-rich relative to the targeted product (e.g., P:Pd = 50:50 in Pd−P), Pd$_5$P$_2$ is the only phase obtained after H$_2$ treatment at 500 °C, suggesting that this phase is the most phosphided phase that can be accessed under high-temperature, reducing conditions. Introduction of excess phosphorus in the direct reduction process by including solid PPh$_3$ upstream of the reactor also led exclusively to Pd$_5$P$_2$.

Thermal gravimetric analysis (TGA) carried out in air on Pd$_5$P$_2$@mSiO$_2$ indicates a weight loss of less than 0.5 wt % is occurring up to 500 °C (see Figure S7 in the Supporting

Information). This suggests that the direct reduction method successfully eliminates the organic matter in Pd−P@SiO$_2$, enabling accessible Pd$_5$P$_2$ particles to be prepared in a single step. The elimination of surfactant is also evident in the nitrogen porosimetry data (representative data shown in Figure S8 in the Supporting Information). The Brunauer−Emmett−Teller (BET) surface area was determined to be 1040 m^2 g^{-1}, whereas the Barrett−Joyner−Halenda BJH adsorption average pore size was 3.7 nm. Mesopores are also evident in high-resolution TEM images (Figure 4a) and are of appropriate size for introduction of molecules such as DBT.
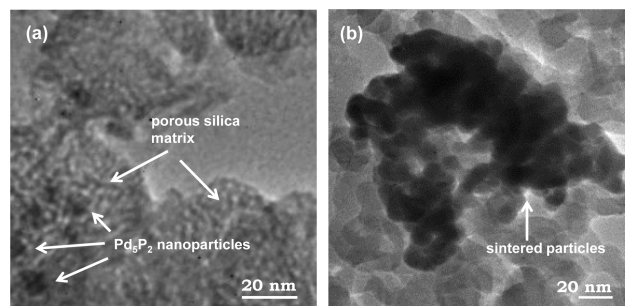
Figure 4. TEM image of (a) Pd$_5$P$_2$@mSiO$_2$ showing the presence of discrete Pd$_5$P$_2$ particles in a porous silica matrix, still present after heating under a reducing environment at 500 °C; (b) sintered particles resultant from heating unencapsulated Pd−P nanoparticles impregnated on to silica by the incipient wetness method under the same conditions as for a.

To demonstrate the importance of the mesoporous silica matrix to prevent sintering, Pd−P nanoparticles were introduced onto an amorphous silica support ((Cab-O-Sil, M-7D grade, 200 m^2/g) using the incipient wetness method and heated under the same conditions with which the Pd−P@mSiO$_2$ samples were treated (5% H$_2$/Ar, 500 °C for 2 h). The resultant particles are significantly sintered, resulting in large crystalline aggregates (Figure 4b). Moreover, the product is not pure; Pd$_3$P is present as a secondary phase (see Figure S9 in the Supporting Information).

Finally, to establish molecule accessibility to the Pd$_5$P$_2$ particles in Pd$_5$P$_2$@mSiO$_2$, and to demonstrate the activity of the catalyst, we conducted CO chemisorption and DBT HDS studies on Pd$_5$P$_2$@mSiO$_2$ (∼9 nm diameter Pd$_5$P$_2$). Dibenzothiophene and alkyl-substituted DBTs are frequently used as model organosulfur compounds for laboratory studies of new hydrotreating catalysts. Carbon monoxide chemisorption experiments were carried out at 0 °C as described elsewhere.[13] The DBT HDS measurements were carried out using a fixed-bed flow reactor operating at 3.0 MPa total pressure and in the temperature range of 250−400 °C. The products of the dibenzothiophene HDS catalytic reaction were collected in 25 °C intervals as a function of temperature. The DBT conversion and HDS selectivity data are shown in Figure 5 for 5 wt % Pd$_5$P$_2$@mSiO$_2$; the DBT conversion increases gradually and consistently with temperature. These activity data prove that active sites on the Pd$_5$P$_2$ particles can be accessed by DBT within the mesoporous silica. The DBT conversion of Pd$_5$P$_2$@mSiO$_2$ is significantly greater than that of a Pd$_5$P$_2$/SiO$_2$ catalyst (calcined precursor) at lower temperatures (<375 °C) and the catalytic activity of the two catalysts is comparable at high temperatures (>375 °C).[13] While Pd$_5$P$_2$/SiO$_2$ prepared from an uncalcined precursor shows higher DBT conversion compared

5405

dx.doi.org/10.1021/am402003g | ACS Appl. Mater. Interfaces 2013, 5, 5403−5407
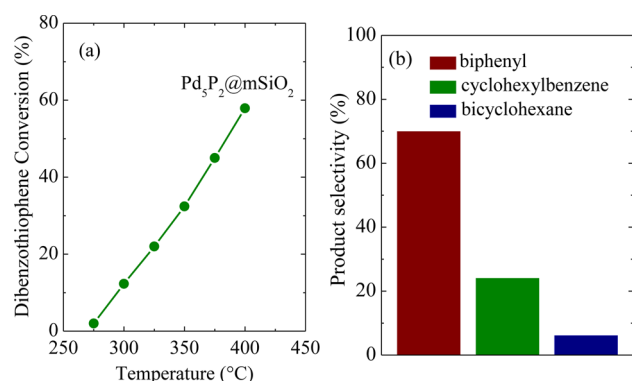
Figure 5. (a) Dibenzothiophene conversion and (b) HDS product selectivity at 325 °C for 5 wt % $Pd_5P_2@mSiO_2$.

to $Pd_5P_2@mSiO_2$, the activity of this catalyst drops significantly at relatively high temperature, suggesting stability may be a problem, in contrast to the $Pd_5P_2@mSiO_2$ catalysts produced here.[13]

The HDS product selectivity of the $Pd_5P_2@mSiO_2$ shows a strong preference for biphenyl, a product of the direct desulfurization (DDS) pathway. Cyclohexylbenzene and bicyclohexane, produced by the hydrogenation (HYD) pathway, comprise the remaining HDS products. Hydrogenated DBTs, intermediates in the HYD pathway to desulfurized products, were detected in the reactor effluent in amounts that decreased with increasing reaction temperature. In contrast, Pd_5P_2/SiO_2 exhibited a product selectivity that slightly favored the products of the HYD pathway.[13] The DBT HDS activities and turnover frequencies (TOFs) for $Pd_5P_2@mSiO_2$ and Pd_5P_2/SiO_2 catalysts,[13] as well as for a conventional sulfided Ni−Mo/Al$_2$O$_3$ catalyst[10] are listed in Table 1.

Table 1. HDS Catalytic Properties

catalyst	CO chem. capacity (μmol/g)	HDS activity[c] (nmol DBT/g·s)	HDS[c] TOF (s^{-1})
$Pd_5P_2@mSiO_2$	4	32	8.0×10^{-3}
Pd_5P_2/SiO_2-calc.[a]	12	2.8	2.3×10^{-4}
Pd_5P_2/SiO_2-uncalc.[a]	3	49	1.6×10^{-2}
Sulf. Ni−Mo/Al$_2$O$_3$[b]	65[d]	143	2.2×10^{-3}

[a]Ref 13]. [b]Ref 10. [c]Measured at 325 °C. [d]O$_2$ chemisorption (μmol O$_2$/g) at −78 °C.

The chemisorption capacities and HDS activities (at 325 °C) were used to calculate TOFs for the Pd phosphide catalysts. The $Pd_5P_2@mSiO_2$ had a TOF that was in between the values determined for the TPR-prepared Pd_5P_2/SiO_2 catalysts, and larger than the TOF of a sulfided Ni−Mo/Al$_2$O$_3$ catalyst. TEM and PXRD analyses done for the post-HDS $Pd_5P_2@mSiO_2$ sample indicates that the particles have not sintered and the Pd_5P_2 phase has been recovered after HDS testing (see Figure S10 in the Supporting Information). Thus, the $Pd_5P_2@mSiO_2$ materials presented here are promising model systems for fundamental studies of HDS catalysis.

In conclusion, we developed a method to synthesize monodisperse, phase-pure, small spherical Pd_5P_2 nanoparticles for the first time. Our approach has the benefit of producing the particles in a mesoporous silica matrix, which reduces sintering at the temperatures needed to crystallize Pd_5P_2, and under the harsh conditions needed to effect hydrodesulfurization of dibenzothiophene. The size-dependent HDS activity, detailed evaluation of products, and study of the mechanism of activity of $Pd_5P_2@mSiO_2$ is underway.

■ ASSOCIATED CONTENT

Ⓢ Supporting Information

Experimental procedures and additional figures (S1−S10) noted in the text. This material is available free of charge via the Internet at http://pubs.acs.org

■ AUTHOR INFORMATION

Corresponding Author

*E-mail: sbrock@chem.wayne.edu.

Notes

The authors declare no competing financial interest.

■ ACKNOWLEDGMENTS

■ REFERENCES

(1) Pawelec, B.; Navarro, R. M.; Campos-Martin, J. M.; Fierro, J. L. G. *Cat. Rev.−Sci. Eng.* **2011**, *1*, 23−42.
(2) Bej, S. K.; Maity, S. K.; Turaga, U. T. *Energy Fuels* **2004**, *18*, 1227−1237.
(3) Schulz, H.; Böhringer, W.; Ousmanov, F.; Waller, P. *Fuel Process. Technol.* **1999**, *61*, 5−41.
(4) Whitehurst, D. D.; Farag, H.; Nagamatsu, T.; Sakanishi, K.; Mochida, I. *Catal. Today* **1998**, *45*, 299−305.
(5) Zepeda, T. A.; Pawelec, B.; Fierro, J. L. G.; Halachev, T. *Appl. Catal., B* **2007**, *71*, 223−236.
(6) Qian, E. W.; Otani, K.; Li, L.; Ishihara, A.; Kabe, T. *J. Catal.* **2004**, *221*, 294−301.
(7) Röthlisberger, A.; Prins, R. *J. Catal.* **2005**, *235*, 229−240.
(8) Niquille-Röthlisberger, A.; Prins, R. *J. Catal.* **2006**, *242*, 207−216.
(9) Kuhn, J. N. In *Catalysis*; Spivey, J. M., Dooley, K. M, Eds.; Royal Society of Chemistry: London, 2011; Vol. 23, p 96−138.
(10) Hayes, J. R.; Bowker, R. H.; Gaudette, A. F.; Smith, M. C.; Moak, C. E.; Nam, C. Y.; Pratum, T. K.; Bussell, M. E. *J. Catal.* **2010**, *276*, 249−258.
(11) Kanda, Y.; Nakata, K.; Temma, C.; Sugioka, M.; Uemichi, Y. *J. Jpn. Pet. Inst.* **2012**, *55*, 108−119.
(12) Kanda, Y.; Temma, C.; Nakata, K.; Kobayashi, T.; Sugioka, M.; Uemichi, Y. *Appl. Catal., A* **2010**, *386*, 171−178.
(13) Bowker, R. H.; Smith, M. C.; Carillo, B. A.; Bussell, M. E. *Top. Catal.* **2012**, *55*, 999−1009.
(14) Guan, Q.; Sun, C.; Li, R.; Li, W. *Catal. Commun.* **2011**, *14*, 114−117.
(15) Prins, R.; Bussell, M. E. *Catal. Lett.* **2012**, *142*, 1413−1436.
(16) Henkes, A. E.; Vasquez, Y.; Schaak, R. E. *J. Am. Chem. Soc.* **2007**, *129*, 1896−1897.
(17) Carenco, S.; Hu, Y.; Florea, I.; Ersen, O.; Boissière, C.; Mézailles, N.; Sanchez, C. *Chem. Mater.* **2012**, *24*, 4134−4145.
(18) Wang, J.; Johnston-Peck, A. C.; Tracy, J. B. *Chem. Mater.* **2009**, *21*, 4462−4467.
(19) Muthuswamy, E.; Savithra, G. H. L.; Brock, S. L. *ACS Nano* **2011**, *5*, 2402−2411.
(20) Moreau, L. M.; Ha, D.-H.; Bealing, C. R.; Zhang, H.; Hennig, R. G.; Robinson, R. D. *Nano Lett.* **2012**, *12*, 4530−4539.
(21) Layan Savithra, G. H.; Bowker, R. H.; Carrillo, B. A.; Bussell, M. E.; Brock, S. L. *Chem. Mater.* **2013**, *25*, 825−833.
(22) Wang, J.; Yang, Q.; Zhang, Z.; Sun, S. *Chem.—Eur. J.* **2010**, *16*, 7916−7924.
(23) Wang, Z.; Zhou, L.; Zhang, M.; Su, M.; Li, W.; Tao, K. *Chem. Asian. J.* **2009**, *4*, 1794−1797.

5406

dx.doi.org/10.1021/am402003g | *ACS Appl. Mater. Interfaces* 2013, 5, 5403−5407

(24) Zafiropoulou, I.; Papagelis, K.; Boukos, N.; Siokou, A.; Niarchos, D.; Tzitzios, V. *J. Phys. Chem. C.* **2010**, *114*, 7582−7585.